Volume 13
Number 48
28 December 2022
Pages 14201–14412

Chemical Science

rsc.li/chemical-science

ISSN 2041-6539

ROYAL SOCIETY OF CHEMISTRY

EDGE ARTICLE

Neso Sojic, Alexander Kuhn *et al.*
Wireless electrochemical light emission in ultrathin 2D nanoconfinements

Chemical Science

ROYAL SOCIETY OF CHEMISTRY

EDGE ARTICLE

View Article Online
View Journal | View Issue

Cite this: *Chem. Sci.*, 2022, **13**, 14277

All publication charges for this article have been paid for by the Royal Society of Chemistry

Received 21st August 2022
Accepted 20th November 2022

DOI: 10.1039/d2sc04670a

rsc.li/chemical-science

Wireless electrochemical light emission in ultrathin 2D nanoconfinements†

S. Mohsen Beladi-Mousavi, Gerardo Salinas, Laurent Bouffier, Neso Sojic * and Alexander Kuhn *

Spatial confinement of chemical reactions or physical effects may lead to original phenomena and new properties. Here, the generation of electrochemiluminescence (ECL) in confined free-standing 2D spaces, exemplified by surfactant-based air bubbles is reported. For this, the ultrathin walls of the bubbles (typically in the range of 100–700 nm) are chosen as a host where graphene sheets, acting as bipolar ECL-emitting electrodes, are trapped and dispersed. The proposed system demonstrates that the required potential for the generation of ECL is up to three orders of magnitude smaller compared to conventional systems, due to the nanoconfinement of the potential drop. This proof-of-concept study demonstrates the key advantages of a 2D environment, allowing a wireless activation of ECL at rather low potentials, compatible with (bio)analytical systems.

Introduction

Confined interfaces have a major impact on chemical or electrochemical reactions in different manners, determined by the dimension of the restricted space and the nature of the interface. Well-known examples are surface-confined systems, redox species in layered materials or in a nanotube, and three-dimensional spaces, where the movement is restricted to the nanometer range.[1] The latter case is often exemplified by mesoporous materials, where the nano-confinement affects the mass transport and the residence time inside a porous electrode.[2] This concept is known as Knudsen-diffusion. The Knudsen theory explains that in certain regimes the probability of collision of target molecules with the electrode is higher than with other molecules.[3] This significantly impacts the electrochemical activity, if the adsorption is not the rate-determining step.[4] This concept has been widely used in complex systems, *e.g.* for imaging and sensing in living cells and for other bioanalytical applications to reduce the required potential or to considerably amplify the current.[5–8]

Electrochemiluminescence (ECL) is a light emission process, triggered by the electrochemical excitation of a luminophore, which found many sensing applications, particularly in clinical analysis and biological research.[9–17] This is due to ECL's high sensitivity and selectivity, exceptionally low background, high linear dynamic range, chemical stability of the luminophore, straightforward conjugation of the ECL-label to biomolecules, and temporal resolution.[18–22] ECL involves an electron transfer process at the surface of an electrode, followed by a sequence of reactions, which eventually leads to the excited state of the luminophore.[23,24] The relaxation of this excited state results in photon emission. The ECL emission is typically generated in a thin layer of an electrolyte solution in the immediate vicinity of an electrode.[25,26] This is due to the (i) spatial limitation of direct electron transfer to nanoscale regions around an activated electrode and (ii) the diffusion limitation of radical species with short lifetimes acting as sacrificial co-reactants.[23,27,28] Thus, the observed light emission is intimately related to the electrode, which is a limiting factor compared to conventional chemiluminescence that occurs in the bulk of a solution.[29–31] This problem has been addressed by using bipolar electrochemistry (BPE) as a wireless approach to generate light in the bulk of a solution.[32,33] Typically, the conductive objects should be well-dispersed in the solution allowing their wireless polarization by the electric field resulting in simultaneous generation of ECL on each individual object. The consequence of this collective behaviour is a strong luminescence in a 3D reaction space, which has opened up new applications *e.g.*, the tracking of (micro)objects.[34–36] Despite the advantages of this system, there are critical issues, which have not been addressed yet:

The polarization voltage (ΔV) generated across a conductive object is proportional to the external electric field (ε), and the dimension of the object (l):

$$\Delta V = \varepsilon \times l \quad (1)$$

Thus, for microparticles, the required electric field is theoretically extremely high, *e.g.*, >1 kV cm^{-1} to obtain a difference

Univ. Bordeaux, CNRS, Bordeaux INP, ISM, UMR 5255, ENSCBP, 33607 Pessac, France. E-mail: kuhn@enscbp.fr; sojic@enscbp.fr

† Electronic supplementary information (ESI) available. See DOI: https://doi.org/10.1039/d2sc04670a

of 2.4 V (the potential difference between the oxidation of the ECL reagents at the anode and reduction of oxygen at the cathode)[32] between the extremities of for example 30 μm objects, and hence not applicable for most systems.[37]

The objects should be well-dispersed in solution, typically *via* a gelation process to prevent sedimentation, aggregation and/or rotation. This limits the application of this system to environments with an appropriate viscosity.[32,37,38]

Exploring novel designs and systems to overcome the abovementioned limitations is of critical importance to develop sensitive detection schemes for biomedical applications, *e.g.*, in bioanalytical assays.[18] Thin reaction environments[39] *e.g.* planar light-emitting electrochemical cells or soap layers have been introduced in conventional electrochemical systems, among others for electroanalysis applications, in which only low potentials are allowed due to the fragility of bubble layers.[39] Ciampi and coworkers reported a higher electrochemical reactivity promoted at the corona of gas bubbles adhering to an electrode surface.[40] Recent studies demonstrated a spatial confinement of voltage drop at nanodimensional spaces *e.g.*, micro/nanopores or at the tip of nanopipets. This resulted in the asymmetric polarization of bipolar electrodes at significantly lower voltages compared to typical BPE systems.[6,7,41]

In this contribution, we were able to achieve ECL emission inside the ultrathin layer of a soap bubble as a 2D reaction space by designing a novel bipolar electrochemical setup that offers a strong confinement (see the schematic illustration in Scheme 1). The thin layer was loaded with 2D graphene microparticles acting as bipolar electrodes, as well as with a luminophore and a co-reactant. The network of graphene sheets placed in the aqueous phase between the surfactant layers of the bubble resulted in well-dispersed microcolloids. This novel system (i) very significantly reduces the applied potential required for ECL by up to three orders of magnitude, due to the confinement of the electric field, (ii) eliminates the precipitation problems of conductive bipolar electrodes since the particles are trapped within the 2D layer of the bubble (Scheme 1) and (iii) guarantees a perfect orientation of the bipolar objects with respect to the electric field lines without using the typical viscous media.

Results and discussion

The bubble consists of sodium dodecyl sulfate (SDS) (surfactant), glycerol, polyoxyethylene (10) cetyl ether (Brij C10), graphene sheets (bipolar electrodes), tris(2,2′-bipyridyl) dichlororuthenium(II) hexahydrate ($Ru(bpy)_3^{2+}$) (luminophore), and 2-(dibutylamino) ethanol (DBAE) (co-reactant) in a phosphate buffer (pH = 7.4). We selected DBAE because it is an efficient co-reactant leading to strong ECL emission, which follows the so-called oxidative/reduction pathway.[42,43] Typically, soap bubbles quickly burst due to a combination of different mechanisms such as liquid evaporation, gravity-induced drainage, and nuclei-induced initiation.[44] The bursting mechanism depends on the composition of the bubble.[45] While some studies suggested exceptionally stable bubbles, they are often based on the protection of the outer layer of the bubble with multiple layers of polymer coatings.[45–47] It is also known that the addition of glycerol to the bubble composition slows down the water evaporation process due to its hygroscopic properties, allowing to compensate for the gradual water loss,[45] whereas the long chain Brij C10 is added to the bubble composition to improve its mechanical stability. Here, the bubble composition has been optimized to ensure a good dispersion of the graphene microparticles in the bubble layer, while providing mechanical stability upon applying a potential, avoiding instantaneous bubble bursting.

Single/few-layer graphene sheets have shown promising potential for various applications due to their unique properties, *e.g.* high electrical conductivity and mechanical flexibility.[48–51] We have previously employed relatively large graphene derivatives, either supported on a substrate[52] or at the liquid/air interface,[53] as bipolar objects and selectively decorated *via* BPE. Also, our recent studies demonstrated the precise tuning of the oxidation degree of graphene oxide sheets *via* BPE.[54] The degree of oxidation was adjusted by controlling the

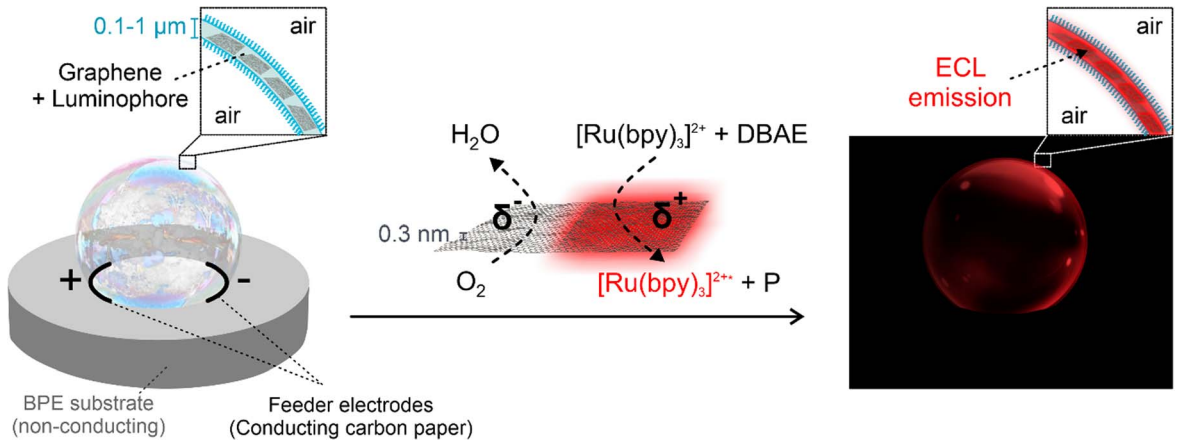

Scheme 1 Schematic overview of ECL occurring within the thin layer of a soap bubble using graphene sheets as bipolar electrodes, in the presence of $Ru(bpy)_3^{2+}$ and 2-(dibutylamino) ethanol (DBAE) as a luminophore and co-reactant, respectively; the bubble images are schematic.

reaction time and the applied electric field. Here, aqueous suspensions of two-dimensional graphene sheets, prepared *via* a scalable wet technique, were directly used. The graphene sheets were obtained by exfoliation of graphite particles with a layered crystal structure *via* a tip sonication procedure[55,56] using the abovementioned bubble solution in the absence of the luminophore and co-reactant (Fig. S1†). Suspensions with 0.1, 1 and 4 mg ml^{-1} graphene concentrations were prepared for this study (see ESI† for more details). The preparation process is designed to achieve single/few layer graphene sheets in samples with low concentration (0.1 mg ml^{-1}). However, when increasing the concentration of graphene sheets (1 and 4 mg ml^{-1}), the formation of stacks of graphene is inevitable, resulting in the generation of microplatelets.

The bubbles were formed and positioned in the bipolar setup between two feeder electrodes using a pipet (see ESI†). The thickness of the walls of these bubbles can be roughly estimated based on the colour pattern at the thin film interface (Fig. 1a).[57] It is evaluated to be 100–700 nm, by matching the colour pattern of the bubble to a reference colour map. Note that the thickness distribution is time dependent as the bubble is not at equilibrium. The images were taken using a digital camera immediately after formation of the bubble with an exposure time of 0.1 s. To enhance the mechanical stability of bubbles, they were cooled down/frozen prior to experiments in order to delay water evaporation. Bubble bursting as a result of water evaporation is accelerated once the potential is applied due to Joule effect. Thus, the container where the bipolar systems are placed is first cooled by pouring liquid nitrogen (LN_2) (Fig. 1b(i)). After evaporation of LN_2, the setup is placed in the container followed by the formation of a bubble *via* air blowing during pipetting (Fig. 1b(ii) and (iii)).

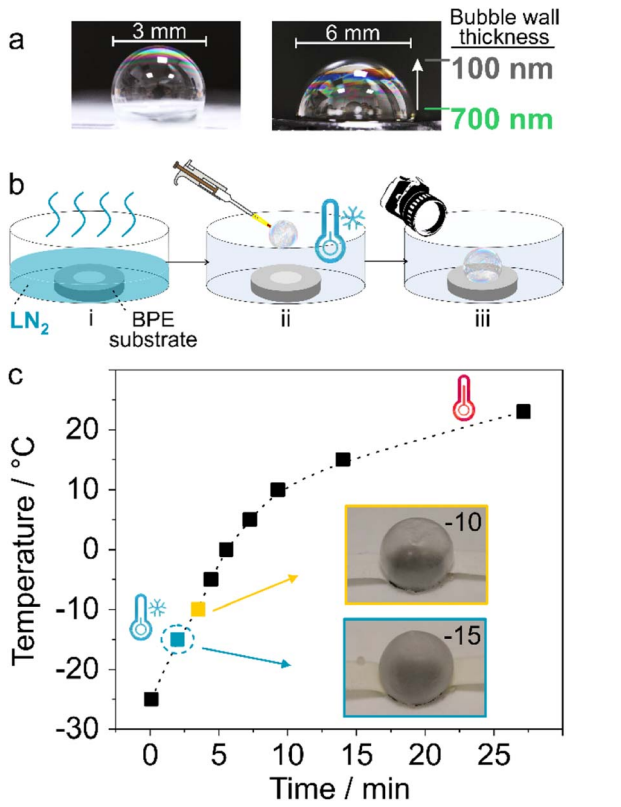

Fig. 1 Bubble formation and stabilization. (a) Images of bubbles of different sizes. (b) Schematic illustrations of the bipolar setup and the tuning of the temperature using liquid nitrogen (LN_2). (c) Temperature of the container of the bipolar setup as a function of time; inset: images of frozen bubbles at −15 °C, and −10 °C, in which the bubbles are stable for ECL measurements. All experiments are measured using bubbles with an initial temperature of −15 °C.

In order to guarantee a stable system, the temperature of the container after LN_2 evaporation is measured. Immediately after the evaporation, a temperature of −24 °C is recorded, which eventually goes back to room temperature within ~30 min (Fig. 1c). The bubbles at −24 °C are not stable and shrinkage and/or breaking is systematically observed (Fig. S2†). However, after 2–5 min, when the temperature rises to −15 °C to −10 °C, the bubbles are stable (Fig. 1c, inset and Fig. S3†). Thus, the experiments were all started at an initial temperature of −15 °C.

In the next step, the generation of ECL in bubbles containing graphene microplatelets as bipolar objects has been explored. As described earlier, extremely high potentials are typically required to provide sufficient polarization of micro/nanosized bipolar objects. Hence, considering the approximate size of the conductive particles in this study *i.e.*, ~2.2 μm (*l*) (Fig. S4†), and the minimal polarization of 2.4 V (ΔV) to couple anodic (oxidation of the ECL reagents) and cathodic reactions (reduction of oxygen) on a carbon substrate,[32] the required electric field (ε) to polarize the particles would be >10 kV cm^{-1} (eqn (1)). Such high values of ε cause several technical problems and are thus not applicable for most ECL systems, including the fragile soap layers. Hence, larger assemblies of conductive objects, as well as confining the potential drop[8] to the ultrathin walls of bubbles, are utilized to reduce the required potential, allowing a sufficient polarization of the conductive objects at lower potentials. Increasing the concentration of the graphene microplatelets is expected to induce aggregation due to hydrophobic interactions. Therefore, different concentrations of graphene (0.1, 1, and 4 mg ml^{-1}) have been examined in order to achieve the formation of larger clusters of graphene sheets *i.e.*, microplatelets in the bubble layer and hence allowing a sufficient polarization even at lower applied electric fields. Dynamic light scattering (DLS) measurements of freshly sonicated samples indicated average cluster sizes of ~1.2, 2.2, and 5 μm for graphene solutions with concentrations of 0.1, 1 and 4 mg ml^{-1}, respectively (Fig. S4†). Moreover, analyzing the concentration of the graphene solutions demonstrated the precipitation of up to 30% of the sheets after 2 min, indicating further colloid formation (see ESI†).

A range of potentials (1–30 V) was applied to the extremities of bubbles formed between feeder electrodes with 6 mm distance (see the ECL setup in Fig. S5†), revealing that they are not stable at ε values higher than 33 V cm^{-1} (Fig. 2a). The accelerated bubble-bursting is related to the liquid evaporation upon applying the electric field. The ECL intensity was measured as a function of the applied electric field for all concentrations of graphene, using the bipolar setup and bubbles at an initial temperature of −15 °C by taking their

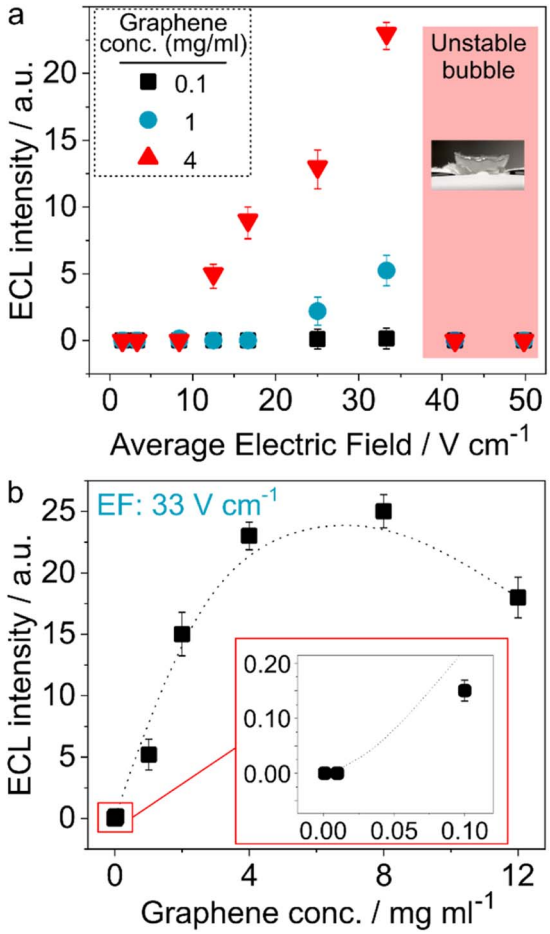

Fig. 2 ECL intensity of bubbles placed in a 6 mm setup. (a) The impact of the magnitude of the average electric field on ECL intensity in the presence of 0.1, 1 and 4 mg ml^{-1} graphene microplatelets. (b) The intensity of ECL in the presence of a wide concentration range of graphene microplatelets (0.001–12 mg ml^{-1}) at a constant electric field of 33 V cm^{-1}.

images in a dark environment with a CCD camera. While no ECL was observed at ε values below 8 V cm^{-1}, 1 and 4 mg ml^{-1} graphene samples showed an ECL response from 12.5 to 25 V cm^{-1}. Remarkably, these values are approximately three orders of magnitude smaller than the theoretical value for a ~2.2 μm bipolar object (>10 kV cm^{-1}), as mentioned earlier. This is attributed to the spatial confinement of the voltage drop in the ultrathin soap bubble layer, leading to a higher driving force. From a conceptual point of view, this experiment can be considered as being an intermediate set-up between open and closed bipolar electrochemistry configurations. In the latter case, a quite small electric field is required since the entire potential drop occurs between the two extremities of the bipolar electrode, as there is no alternative current path. In contrast, in the completely open set-up only a small fraction of the current goes through the bipolar object because there is a strong competition with the current flow through the surrounding 3D electrolyte environment and therefore higher driving forces in terms of voltage have to be applied to generate the same current as the one flowing through the bipolar object in the closed set-up. The parasitic current flow is drastically reduced in a 2D setup, thus leading to a lower overall potential difference to drive the redox reactions at the bipolar electrodes.

Another explanation for the much lower electric fields might be simply the aggregation of graphene particles leading to bigger clusters which can be polarized more easily. However, the solutions for preparing the bubble and the ones used for DLS measurements are very similar. Both solutions are sonicated in an identical way and the experiments (DLS and bubble generation) are performed immediately after sonication. Moreover, the bubbles are immediately frozen after generation. Hence, the dispersion of graphene in the bubbles should be very similar compared to the DLS measurements. Nevertheless, the possibility of aggregation of particles after applying potential, along with the melting of the bubble wall, must be considered. Theoretical calculations show that activating bipolar ECL at 12.5 V cm^{-1} (Fig. 2) would require conducting objects with a minimum size of 2 mm. Considering the size of the setup (3 and 6 mm), a homogeneous distribution of luminescence, such as the one shown in Fig. 3b, would not be possible if 2 mm long aggregates were the emitters, because light emission should then only occur at the anodic extremity of such objects. This would lead only to a very small number of light emitting spots, distributed randomly over the bubble surface. Moreover, analysis of the pixels of the corresponding images demonstrate that the size of each pixel is *ca.* 1.4 μm. Except in bubbles obtained from a 4 mg ml^{-1} graphene solution, for which 0.1–0.2 mm shiny spots are observed, the 1 and 2 mg ml^{-1} bubbles do not show any spot bigger than the pixels' size. Even in the case of the 4 mg ml^{-1} solution, the size of the light emitting spots is too small to be explained by a "normal" potential drop. This confirms that the size of emitting particles must be very small and that the ECL activation at low potentials is strictly due to the spatial confinement.

Furthermore, the ECL intensity was significantly larger for the 4 mg ml^{-1} samples, which is attributed to the more frequent formation of big colloidal particles (Fig. 2a). This affects ECL intensity not only because of the presence of larger colloids, but the bigger size of bipolar electrodes under nanoconfinement enhances also the collision frequency of target molecules with the electrodes. The ECL of bubbles, located between feeder electrodes with a 3 mm distance, could be triggered already for lower potentials, and higher intensities were observed (Fig. S6†). This is due to the direct relation between the applied voltage and the distance between the feeder electrodes according to eqn (S1).†[58] It should be noted that the charge transfer between feeder electrodes is occurring over the entire interface with the bubble and hence at a slightly different electric field strength depending on the position on the bubble. At the bottom (in the plane of the feeder electrodes), ECL intensity might be stronger due to shorter charge migration distance, however this part is hidden inside the ECL setup and is therefore not visualized. Hence, an average for the electric field is calculated based on an average distance between feeder electrodes through the bubble wall, assuming that the distance between feeder electrodes at top and bottom part of bubble is

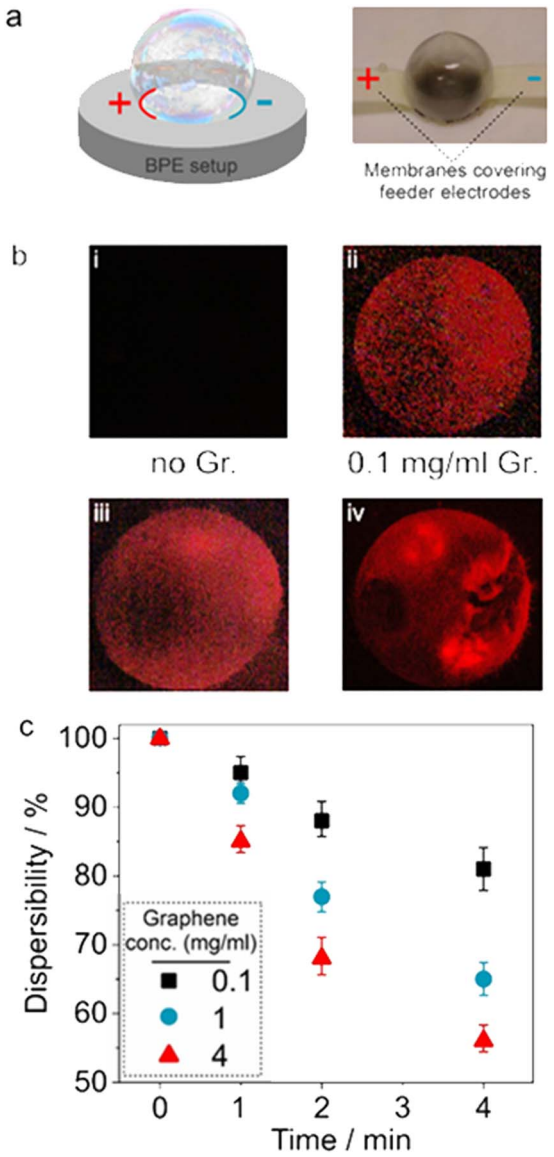

Fig. 3 The correlation between ECL and the aggregation of graphene sheets; (a) schematic illustration of a bipolar electrochemical setup (left) and an image of an initially frozen bubble at −15 °C placed between feeder electrodes that are covered with a membrane to avoid their direct contact with the bubble (right, 6 mm bubble) (see also Fig. S5†). (b) Images of the light-emitting bubbles (taken from the upper side angle, as shown in Fig. 1b) with 0.1, 1, and 4 mg ml^{-1} graphene content; 6 mm bubbles. (c) Dispersibility of graphene sheets in the original solution, which was used to prepare the bubbles, during 4 minutes after bath sonication.

equal. In order to allow for a better comparison of the different experiments, the ECL intensities were all measured from images captured after 5 seconds of applying potential, with 5 seconds exposure time.

To provide a better insight into the effect of graphene concentration on the ECL intensity, a more detailed study, using a wide concentration range of graphene from 0.001 to 12 mg ml^{-1} for a constant ε value (33 V cm^{-1}), was performed (Fig. 2b). While only weak luminescence was recorded with a 0.1 mg ml^{-1} solution, the intensity significantly increased for 1 mg ml^{-1} and reached its maximum value at 4–8 mg ml^{-1}. Moreover, the lifetime of bubbles with 12 mg ml^{-1} was shorter and bubbles containing even higher concentrations were unstable, which did not allow recording their ECL response.

The images of the illuminating bubbles and the experimental setup are shown in Fig. 3 and S5.† The ECL emitted by the spherical bubbles (Fig. 3b) was captured for a given electric field (33 V cm^{-1}) in a 6 mm setup. The same behaviour is recorded in setups in which two interconnected bubbles are placed between the feeder electrodes (Fig. S7†). While no ECL was observed for bubbles generated from solutions without graphene (i), a quite uniform luminescence was detected for bubbles containing a low concentration of graphene moieties (ii) attributed to the homogeneous distribution of the bipolar microobjects. Further increasing the concentration of graphene microplatelets leads to a globally stronger emission and the appearance of hot spots with locally higher ECL intensities (iii and iv). This can be explained by the formation of larger aggregates of graphene at higher concentrations, as well as the formation of a localized nanoconfinement within the colloidal graphene aggregates and at their interface with the bubble walls, acting similar to a mesoporous structure.[1]

It should be noted that the polarization potential is proportional to the size of the bipolar electrodes, which under these conditions have a certain polydispersity (eqn (1)). To confirm the aggregation of the bipolar objects, the final concentrations of graphene microplatelets remaining in the supernatant of suspensions with initial concentrations of 0.1, 1, and 4 mg ml^{-1} were measured during 4 minutes after a sonication step (Fig. 3c, see ESI† for more details). As expected, a faster precipitation was observed for solutions with higher concentrations, indicating the lower graphene dispersibility and thus a more rapid aggregation/precipitation.[54] The bubbles were generated from solutions that were freshly sonicated. The precipitation rate for the 1 and particularly 4 mg ml^{-1} solution is significantly higher than for the more diluted samples (Fig. 3c). This is reflected by the more localized ECL emission of bubbles prepared with these higher concentrations (Fig. 3b(iv)).

Finally, the ECL response of a bubble containing 1 mg ml^{-1} graphene along its lifetime has been analyzed when applying 33 V cm^{-1}, while imaging with 5 seconds exposure time (Fig. 4). The bubble was generated and positioned in the bipolar setup, which then was placed in a container with a temperature of ∼−15 °C. It should be noted that while the temperature of the bubble's surrounding is initially below the freezing point of water, the bubble temperature is expected to be >0 °C during ECL measurements upon applying the potential due to the Joule effect.[59] The ECL intensity and distribution is illustrated for a period of 30 s in Fig. 4. As it can be seen from Fig. 4, ECL is already observed after only 5 seconds. This demonstrates that the bubble cannot be any longer in the frozen state as ion transport is required for the electrochemical reactions. The image captured after applying potential for 20 s shows some holes at the top part of bubbles, which demonstrates that the bubble walls are liquid, but the membrane is still at

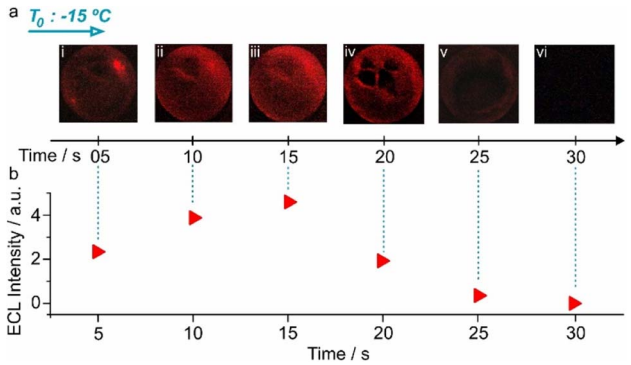

Fig. 4 ECL of a bubble during its lifetime. ECL images of a bubble (taken from the upper side angle, as shown in Fig. 1b), kept in a −15 °C environment, for 30 seconds with 5 seconds exposure time during the imaging (a) and the corresponding ECL intensities (b). 6 mm bubbles.

a temperature which is low enough to stabilize these defects due to a sufficiently high viscosity.

The first image exhibited areas on the bubble with considerably higher ECL intensities (Fig. 4a(i)). This is because frozen areas still exist and light is only produced through a percolation path along the particles where the temperature is already >0 °C. Once the entire bubble is at >0 °C, the light emission becomes very homogeneous (Fig. 4a(ii) and (iii)). Notably, the ECL intensity was very pronounced during the first 15 seconds, before a partial breaking of the bubble starts, leading to lower intensities (Fig. 4a(iv), (v) and b), until no luminescence is observed (Fig. 4a(vi) and b). Note that if no potential is applied, the bubbles are stable for >10 min (Fig. S3†). The initial enhanced intensity is related to the completion of the phase change of bubble walls from solid to liquid, which results in a lower resistance at the interface between the bubble and the membranes covering the electrodes, as well as an enhanced mass transfer in the surroundings of the bipolar objects.

Conclusions

In conclusion, this study demonstrates for the first time the possibility to trigger ECL in an original confined 2D space *i.e.* inside the ultrathin walls of soap bubbles, loaded with graphene sheets/microplatelets as bipolar objects. Despite the small size of these bipolar electrodes (<5 μm), it is possible to activate ECL at potentials which are three orders of magnitude smaller than the theoretical value. This exceptional behavior is attributed on the one hand to the formation of larger 2D aggregates of graphene sheets in the aqueous phase of the soap layer, due to hydrophobic interactions. On the other hand, the confinement itself allows focusing the potential drop precisely in the plane of the graphene sheets, which drastically decreases bypass currents that otherwise would dominate the current flow in an open 3D configuration. This makes the set-up comparable with a closed bipolar electrochemical cell, in which the polarization of conducting objects is much easier.[58] In addition, this particular electrochemical setup traps the conductive objects and thus eliminates one of the challenges of performing BE in bulk solutions concerning the conservation of the orientation of the bipolar objects, which typically requires the use of a gel electrolyte. The proposed system, taking advantage of the nanoconfinement in an original setup, offers the generation of ECL at exceptionally low potentials *via* a wireless electrochemical approach, which might open-up new possibilities for bioanalytical applications. While this proof-of-concept study is focused on the elaboration of such a 2D nanoconfinement in the walls of a pre-frozen soap bubble, the ECL reaction itself is occurring in the liquid state and the bubble walls are solely intended to provide a thin 2D layer. This demonstrates that the main requirement for minimizing the driving force in terms of input potential is the presence of the nanoconfinement. Therefore, these findings can be generalized and expanded to other systems that are able to provide a similar confined environment, but do not necessarily require low temperatures, and therefore become also compatible with biological systems.

Data availability

Additional data can be obtained from the corresponding author upon request.

Author contributions

S. Mohsen Beladi-Mousavi: investigation, methodology, formal analysis, visualization, writing – original draft, writing – review & editing. Gerardo Salinas: investigation, formal analysis, writing – original draft. Laurent Bouffier: conceptualization, writing – review & editing. Neso Sojic: conceptualization, supervision, writing – review & editing, Alexander Kuhn: conceptualization, supervision, funding acquisition, writing – review & editing.

Conflicts of interest

The authors declare no competing financial interests.

Acknowledgements

The work has been funded by the European Research Council under the European Union's Horizon 2020 research and innovation program (grant agreement no 741251, ERC Advanced grant ELECTRA).

References

1 M. Jaugstetter, N. Blanc, M. Kratz and K. Tschulik, *Chem. Soc. Rev.*, 2022, **51**, 2491–2543.
2 A. J. Medford, A. Vojvodic, J. S. Hummelshøj, J. Voss, F. Abild-Pedersen, F. Studt, T. Bligaard, A. Nilsson and J. K. Nørskov, *J. Catal.*, 2015, **328**, 36–42.
3 J. H. Bae, J.-H. Han and T. D. Chung, *Phys. Chem. Chem. Phys.*, 2012, **14**, 448–463.
4 H. S. White and K. McKelvey, *Curr. Opin. Electrochem.*, 2018, **7**, 48–53.

5 Y.-L. Ying, Y.-X. Hu, R. Gao, R.-J. Yu, Z. Gu, L. P. Lee and Y.-T. Long, *J. Am. Chem. Soc.*, 2018, **140**, 5385–5392.
6 R.-J. Yu, Y.-L. Ying, R. Gao and Y.-T. Long, *Angew. Chem., Int. Ed.*, 2019, **58**, 3706–3714.
7 Y. Wang, R. Jin, N. Sojic, D. Jiang and H.-Y. Chen, *Angew. Chem., Int. Ed.*, 2020, **59**, 10416–10420.
8 A. Ismail, S. Voci, P. Pham, L. Leroy, A. Maziz, L. Descamps, A. Kuhn, P. Mailley, T. Livache, A. Buhot, T. Leichlé, A. Bouchet-Spinelli and N. Sojic, *Anal. Chem.*, 2019, **91**, 8900–8907.
9 Z. Liu, W. Qi and G. Xu, *Chem. Soc. Rev.*, 2015, **44**, 3117–3142.
10 S. Rebeccani, A. Zanut, C. I. Santo, G. Valenti and F. Paolucci, *Anal. Chem.*, 2022, **94**, 336–348.
11 X. Ma, W. Gao, F. Du, F. Yuan, J. Yu, Y. Guan, N. Sojic and G. Xu, *Acc. Chem. Res.*, 2021, **54**, 2936–2945.
12 C. Ma, Y. Cao, X. Gou and J.-J. Zhu, *Anal. Chem.*, 2020, **92**, 431–454.
13 H. Qi and C. Zhang, *Anal. Chem.*, 2020, **92**, 524–534.
14 J. Dong, Y. Lu, Y. Xu, F. Chen, J. Yang, Y. Chen and J. Feng, *Nature*, 2021, **596**, 244–249.
15 G. Valenti, E. Rampazzo, S. Kesarkar, D. Genovese, A. Fiorani, A. Zanut, F. Palomba, M. Marcaccio, F. Paolucci and L. Prodi, *Coord. Chem. Rev.*, 2018, **367**, 65–81.
16 M. W. Glasscott and J. E. Dick, *J. Phys. Chem. Lett.*, 2020, **11**, 4803–4808.
17 M. W. Glasscott, S. Voci, P. J. Kauffmann, A. I. Chapoval and J. E. Dick, *Langmuir*, 2021, **37**, 2907–2912.
18 J. Zhang, S. Arbault, N. Sojic and D. Jiang, *Annu. Rev. Anal. Chem.*, 2019, **12**, 275–295.
19 W. Gu, H. Wang, L. Jiao, Y. Wu, Y. Chen, L. Hu, J. Gong, D. Du and C. Zhu, *Angew. Chem., Int. Ed.*, 2020, **59**, 3534–3538.
20 Y. Wang, W. Guo, Q. Yang and B. Su, *J. Am. Chem. Soc.*, 2020, **142**, 1222–1226.
21 S. Chen, H. Ma, J. W. Padelford, W. Qinchen, W. Yu, S. Wang, M. Zhu and G. Wang, *J. Am. Chem. Soc.*, 2019, **141**, 9603–9609.
22 J. Dong, Y. Xu, Z. Zhang and J. Feng, *Angew. Chem., Int. Ed.*, 2022, **61**, e202200187.
23 A. Zanut, A. Fiorani, S. Canola, T. Saito, N. Ziebart, S. Rapino, S. Rebeccani, A. Barbon, T. Irie, H.-P. Josel, F. Negri, M. Marcaccio, M. Windfuhr, K. Imai, G. Valenti and F. Paolucci, *Nat. Commun.*, 2020, **11**, 2668.
24 M. Hesari and Z. Ding, *Nat. Protoc.*, 2021, **16**, 2109–2130.
25 Y. Zu, Z. Ding, J. Zhou, Y. Lee and A. J. Bard, *Anal. Chem.*, 2001, **73**, 2153–2156.
26 W. Miao, J.-P. Choi and A. J. Bard, *J. Am. Chem. Soc.*, 2002, **124**, 14478–14485.
27 M. Sentic, M. Milutinovic, F. Kanoufi, D. Manojlovic, S. Arbault and N. Sojic, *Chem. Sci.*, 2014, **5**, 2568–2572.
28 W. Guo, P. Zhou, L. Sun, H. Ding and B. Su, *Angew. Chem., Int. Ed.*, 2021, **60**, 2089–2093.
29 M. Yang, J. Huang, J. Fan, J. Du, K. Pu and X. Peng, *Chem. Soc. Rev.*, 2020, **49**, 6800–6815.
30 D. Cui, J. Li, X. Zhao, K. Pu and R. Zhang, *Adv. Mater.*, 2020, **32**, 1906314.
31 J. Yang, W. Yin, R. Van, K. Yin, P. Wang, C. Zheng, B. Zhu, K. Ran, C. Zhang, M. Kumar, Y. Shao and C. Ran, *Nat. Commun.*, 2020, **11**, 4052.
32 M. Sentic, S. Arbault, L. Bouffier, D. Manojlovic, A. Kuhn and N. Sojic, *Chem. Sci.*, 2015, **6**, 4433–4437.
33 F. Mavré, K.-F. Chow, E. Sheridan, B.-Y. Chang, J. A. Crooks and R. M. Crooks, *Anal. Chem.*, 2009, **81**, 6218–6225.
34 G. Salinas, I.-A. Pavel, N. Sojic and A. Kuhn, *ChemElectroChem*, 2020, **7**, 4853–4862.
35 M. Sentic, G. Loget, D. Manojlovic, A. Kuhn and N. Sojic, *Angew. Chem., Int. Ed.*, 2012, **51**, 11284–11288.
36 G. Salinas, A. L. Dauphin, S. Voci, L. Bouffier, N. Sojic and A. Kuhn, *Chem. Sci.*, 2020, **11**, 7438–7443.
37 A. de Poulpiquet, B. Diez-Buitrago, M. Milutinovic, B. Goudeau, L. Bouffier, S. Arbault, A. Kuhn and N. Sojic, *ChemElectroChem*, 2016, **3**, 404–409.
38 J. Li and E. Wang, in *Analytical Electrogenerated Chemiluminescence: From Fundamentals to Bioassays*, The Royal Society of Chemistry, 2020, pp. 176–199, DOI: **10.1039/9781788015776-00176**.
39 K. J. Vannoy, N. E. Tarolla, P. J. Kauffmann, R. B. Clark and J. E. Dick, *Anal. Chem.*, 2022, **94**, 6311–6317.
40 Y. B. Vogel, C. W. Evans, M. Belotti, L. Xu, I. C. Russell, L.-J. Yu, A. K. K. Fung, N. S. Hill, N. Darwish, V. R. Gonçales, M. L. Coote, K. Swaminathan Iyer and S. Ciampi, *Nat. Commun.*, 2020, **11**, 6323.
41 R. Hao, Y. Fan and B. Zhang, *J. Am. Chem. Soc.*, 2017, **139**, 12274–12282.
42 L. Bouffier and N. Sojic, in *Analytical Electrogenerated Chemiluminescence: From Fundamentals to Bioassays*, The Royal Society of Chemistry, 2020, pp. 1–28, DOI: **10.1039/9781788015776-00001**.
43 X. Liu, L. Shi, W. Niu, H. Li and G. Xu, *Angew. Chem., Int. Ed.*, 2007, **46**, 421–424.
44 G. Debrégeas, P. G. de Gennes and F. Brochard-Wyart, *Science*, 1998, **279**, 1704–1707.
45 A. Roux, A. Duchesne and M. Baudoin, *Phys. Rev. Fluids*, 2022, **7**, L011601.
46 P. S. Bhosale, M. V. Panchagnula and H. A. Stretz, *Appl. Phys. Lett.*, 2008, **93**, 034109.
47 B. Laborie, F. Lachaussée, E. Lorenceau and F. Rouyer, *Soft Matter*, 2013, **9**, 4822–4830.
48 S. M. Beladi-Mousavi, B. Khezri, S. Matějková, Z. Sofer and M. Pumera, *Angew. Chem., Int. Ed.*, 2019, **58**, 13340–13344.
49 S. M. Beladi-Mousavi, J. Klein, M. Ciobanu, S. Sadaf, A. M. Mahmood and L. Walder, *Small*, 2021, **17**, 2103885.
50 S. M. Beladi-Mousavi, S. Sadaf, A.-K. Hennecke, J. Klein, A. M. Mahmood, C. Rüttiger, M. Gallei, F. Fu, E. Fouquet, J. Ruiz, D. Astruc and L. Walder, *Angew. Chem., Int. Ed.*, 2021, **60**, 13554–13558.
51 P. S. Toth, A. T. Valota, M. Velický, I. A. Kinloch, K. S. Novoselov, E. W. Hill and R. A. W. Dryfe, *Chem. Sci.*, 2014, **5**, 582–589.
52 L. Zuccaro, A. Kuhn, M. Konuma, H. K. Yu, K. Kern and K. Balasubramanian, *ChemElectroChem*, 2016, **3**, 372–377.
53 P. Kankla, P. Luksirikul, P. Garrigue, B. Goudeau, L. Bouffier and A. Kuhn, *Adv. Mater. Interfaces*, 2022, **9**, 2200304.

54 S. M. Beladi-Mousavi, G. Salinas, N. Antonatos, V. Mazanek, P. Garrigue, Z. Sofer and A. Kuhn, *Carbon*, 2022, **191**, 439–447.
55 S. M. Beladi-Mousavi, Y. Ying, J. Plutnar and M. Pumera, *Small*, 2020, **16**, 2002037.
56 S. M. Beladi-Mousavi, J. Plutnar and M. Pumera, *ACS Appl. Mater. Interfaces*, 2020, **12**, 55936–55944.
57 Y. D. Afanasyev, G. T. Andrews and C. G. Deacon, *Am. J. Phys.*, 2011, **79**, 1079–1082.
58 L. Bouffier, D. Zigah, N. Sojic and A. Kuhn, in *Encyclopedia of Electrochemistry*, 2022, ed. A. J. Bard, DOI: **10.1002/9783527610426.bard030112**.
59 P. Personne and J. F. Gayet, *J. Appl. Meteorol. Climatol.*, 1988, **27**, 101–114.